Optimal control of quantum gates and suppression of decoherence in a system of interacting two-level particles

Matthew Grace[1], Constantin Brif[1], Herschel Rabitz[1],
Ian A. Walmsley[2], Robert L. Kosut[3], and Daniel A. Lidar[4]

[1] Department of Chemistry, Princeton University, Princeton, New Jersey 08544

[2] Department of Physics, University of Oxford, Oxford OX1 3PU, UK

[3] SC Solutions, Inc., 1261 Oakmead Parkway, Sunnyvale, CA 94085

[4] Departments of Chemistry, Electrical Engineering, and Physics, University of Southern California, Los Angeles, CA 90089

E-mail: `mgrace@princeton.edu`, `cbrif@princeton.edu`, `hrabitz@princeton.edu`, `walmsley@physics.ox.ac.uk`, `kosut@scsolutions.com`, and `lidar@usc.edu`

Abstract. Methods of optimal control are applied to a model system of interacting two-level particles (e.g., spin-half atomic nuclei or electrons or two-level atoms) to produce high-fidelity quantum gates while simultaneously negating the detrimental effect of decoherence. One set of particles functions as the quantum information processor, whose evolution is controlled by a time-dependent external field. The other particles are not directly controlled and serve as an effective environment, coupling to which is the source of decoherence. The control objective is to generate target one- and two-qubit unitary gates in the presence of strong environmentally-induced decoherence and under physically motivated restrictions on the control field. The quantum-gate fidelity, expressed in terms of a novel state-independent distance measure, is maximized with respect to the control field using combined genetic and gradient algorithms. The resulting high-fidelity gates demonstrate the feasibility of precisely guiding the quantum evolution via optimal control, even when the system complexity is exacerbated by environmental coupling. It is found that the gate duration has an important effect on the control mechanism and resulting fidelity. An analysis of the sensitivity of the gate performance to random variations in the system parameters reveals a significant degree of robustness attained by the optimal control solutions.

1. Introduction

The transfer of information between elements of a quantum computational system requires the use of entangling quantum interactions [1]. Undesired interactions between the system and its surroundings can destroy quantum coherences and thus are a critical obstacle to successful quantum computation (QC). The feasibility of creating high-fidelity quantum gates in the presence of environmentally-induced decoherence is one of the most important problems to overcome for practical QC. In particular, in spin-based solid-state realizations of QC [2, 3, 4, 5] one encounters a difficult task of effectively separating a multiparticle quantum system into interacting and non-interacting components.

Quantum error correction (QEC) enables fault-tolerant QC [6], but only when the errors in quantum gate operations are sufficiently small [7]. Therefore, it is very important to decrease the errors caused by decoherence. This problem has inspired significant interest in various methods of decoherence management, including the use of decoherence-free subspaces and noiseless subsystems [8, 9, 10, 11, 12], quantum dynamical decoupling [13, 14, 15, 16, 17, 18, 19, 20], schemes based on stochastic control [21], optimal control techniques [22, 23, 24, 25, 26, 27], and multilevel encoding of logical states [28].

The method of optimal control [29, 30] enables managing the dynamics of complex quantum systems in a very precise and specific manner and therefore is especially useful in QC. In addition to applications to the problem of dynamical suppression of decoherence [22, 23, 24, 25, 26, 27], optimal control theory (OCT) [31, 32] was also successfully used to design unitary quantum gates in closed systems [33, 34, 35, 36, 37]. The optimal control of quantum gates in the presence of decoherence still remains to be fully explored. In [28] we previously considered the optimal control of quantum gates for qubits encoded in multilevel subspaces; this method makes quantum gates immune to mixing and decoherence that occur within the encoding subspaces. Recent works [38, 39] developed specific techniques, involving optimizations over sets of controls operating in pre-designed "weak-decoherence" subspaces. In the present paper we propose a different approach in which the full power of OCT is used to generate the target gate with the highest possible fidelity while simultaneously suppressing strong decoherence induced by coupling to a multiparticle environment. This method does not rely on any special pre-design of the system parameters to avoid or weaken decoherence (e.g., using multiple levels as in [28], tunable inter-qubit couplings as in [38], or auxiliary qubits as in [39]); the only control used in the present approach is a time-dependent external field.

A similar OCT-based approach was recently used [40] to design quantum gates for solid-state qubits in the presence of decoherence. However, the objective in [40] was to optimize a purity-dependent quality factor (or, in [38], the purity itself), instead of the actual gate fidelity. In the present work we demonstrate that although improving the purity of the quantum information processor (QIP) is necessary for performing a high-fidelity quantum gate, it is not sufficient. Even if the QIP is completely decoupled from

its environment at a given time, this does not ensure that the desired gate operation will be performed at the decoupling time. Therefore, we optimize a gate fidelity [41] which directly measures the distance between the target quantum gate of the QIP and the actual transformation of the composite system. Optimization techniques were also applied recently to QEC [42, 43]. In contrast to QEC, our approach does not require ancilla qubits and is not limited to the weak decoherence regime. The optimal control of quantum gates can potentially be used in conjunction with QEC to achieve fault tolerance with an improved threshold.

In this work, we consider a model system composed of interacting two-level particles, for example, spin-half atomic nuclei or electrons or two-level atoms. A small set of particles serve as qubits in the QIP; the rest of the particles serve as an effective environment. The qubits are directly controlled by a time-dependent external field, while the environmental particles do not directly couple to the field. The control objective is to generate target quantum gates in the QIP with the highest possible fidelity. The optimal control field must perform the desired gate operation while simultaneously suppressing the qubit-environment interaction and restoring lost coherence to the QIP. This model is sufficiently simple to allow for a full numerical treatment of the entire composite system, and the results are relevant to important physical applications, in particular, to spin-based solid-state realizations of quantum gates [2, 3, 4, 5]. For example, our model bears a similarity to systems in which an electron spin (or a pair of electron spins) is coupled to a nuclear spin bath [5, 44, 45]. Coherent manipulation of electron spins via rapid electrical control of the exchange interaction has been successfully demonstrated in such systems [5]. The analysis reported in the present work indicates that the employment of the optimal control methods may increase the effectiveness of coherent management of coupled spin dynamics.

The paper is organized as follows. Section 2 presents the model (including an explicit matrix form for the simplest case of one qubit coupled to a one-particle environment) and schemes of multiparticle couplings. In section 3, we consider a distance measure that quantifies the fidelity of quantum gates. This fidelity is independent of the initial state and is evaluated directly from the evolution operator of the composite system. Section 4 investigates the dynamics of decoherence in the uncontrolled system for various values of system parameters. In order to fully explore the utility of OCT, we select a set of parameters that enhances the loss of coherence in the uncontrolled system. In section 5, we describe in detail the genetic and gradient optimization algorithms. The results obtained with the optimal controls are presented and discussed in section 6. Section 7 investigates the robustness of optimal solutions to uncertainties in the system parameters. Finally, section 8 concludes with a summary of the results and discusses future directions.

2. The model system

We use a model of N interacting two-level particles (e.g., spin-half particles or two-level atoms), which are divided into the QIP, composed of m qubits, and an n-particle environment ($N = m + n$). The qubits are directly coupled to a time-dependent external control field, while the environment is not directly controlled and is managed only through its interaction with the qubits. The evolution of the composite system of qubits and environment is treated in an exact quantum-mechanical manner, without either approximating the dynamics by a master equation or using a perturbative analysis based on the weak coupling assumption. The Hamiltonian for the composite controlled system, $H = H_0 + H_C + H_{\text{int}}$, has the form ($\hbar = 1$)

$$H = \sum_{i=1}^{N} \omega_i S_{iz} - \sum_{i=1}^{m} \mu_i C(t) S_{ix} - \sum_{i=1}^{N-1} \sum_{j>i}^{N} \gamma_{ij} \mathbf{S}_i \cdot \mathbf{S}_j. \tag{1}$$

Here, $\mathbf{S}_i = (S_{ix}, S_{iy}, S_{iz})$ is the spin operator for the ith particle ($\mathbf{S}_i = \frac{1}{2}\boldsymbol{\sigma}_i$, in terms of the Pauli matrices), H_0 is the sum over the free Hamiltonians $\omega_i S_{iz}$ for all N particles (ω_i is the transition angular frequency for the ith particle), H_C specifies the coupling between the m qubits and the time-dependent control field $C(t)$ (μ_i are the dipole moments), and H_{int} represents the Heisenberg exchange interaction between the particles (γ_{ij} is the coupling constant for the ith and jth particles). This model is particularly relevant to spin-based solid-state realizations of quantum gates [2, 3, 4, 5].

Now consider the simplest case of one qubit and a one-particle environment ($m = n = 1$) in more detail. The Hamiltonian in this case is:

$$H = \omega_1 S_{1z} + \omega_2 S_{2z} - \mu C(t) S_{1x} - \gamma \mathbf{S}_1 \cdot \mathbf{S}_2, \tag{2}$$

where $\gamma = \gamma_{12}$. We use the orthonormal basis:

$$|1\rangle = |+\rangle_1 \otimes |+\rangle_2, \quad |2\rangle = |+\rangle_1 \otimes |-\rangle_2, \quad |3\rangle = |-\rangle_1 \otimes |+\rangle_2, \quad |4\rangle = |-\rangle_1 \otimes |-\rangle_2, \tag{3}$$

where $S_{iz}|\pm\rangle_i = \pm\frac{1}{2}|\pm\rangle_i$. The Hamiltonian (2) in the basis (3) has the following matrix form:

$$H = \frac{1}{2} \begin{pmatrix} \omega_1 + \omega_2 - \frac{1}{2}\gamma & 0 & -\mu C(t) & 0 \\ 0 & \omega_1 - \omega_2 + \frac{1}{2}\gamma & -\gamma & -\mu C(t) \\ -\mu C(t) & -\gamma & \omega_2 - \omega_1 + \frac{1}{2}\gamma & 0 \\ 0 & -\mu C(t) & 0 & -\omega_1 - \omega_2 - \frac{1}{2}\gamma \end{pmatrix}. \tag{4}$$

In addition to the simplest case of a two-particle system described above, we also consider situations where one qubit is coupled to a multiparticle environment ($m = 1$ and $n = 2, 4, 6$). For $m = 1$, the coupling constants are given by

$$\gamma_{ij} = \begin{cases} \gamma, & \text{for } i = 1 \text{ and } j = 2, \ldots, N, \\ 0, & \text{for } 2 \leq i \leq N, \end{cases} \tag{5}$$

which means that the qubit interacts with each environmental particle with the same coupling constant γ, and the environmental particles are not directly coupled to each other. For $n = 2$, the system can be modeled by a linear chain with the qubit q_1 at the center, equally coupled to both environmental particles e_2 and e_3:

$$e_2 \longleftrightarrow q_1 \longleftrightarrow e_3 \tag{6}$$

For $n = 4$, the system can be modeled by a two-dimensional lattice with the qubit q_1 at the center, equally coupled to four environmental particles $\{e_2, \ldots, e_5\}$:

$$
\begin{array}{c}
e_4 \\
\updownarrow \\
e_2 \longleftrightarrow q_1 \longleftrightarrow e_3 \\
\updownarrow \\
e_5
\end{array}
\tag{7}
$$

Similarly, for $n = 6$, the system can be modeled by a three-dimensional lattice with the qubit at the center, coupled to six environmental particles. In these lattices, it is assumed that the Heisenberg interactions decay exponentially with distance [2], and therefore environmental particles on the vertices of the square ($n = 4$) and cube ($n = 6$) are neglected.

A different model with nearest-neighbor couplings is also considered in the case of $n = 4$. The system is modeled by a linear chain of particles, with the qubit at the center and each particle coupled only to its nearest neighbors with the same coupling constant γ:

$$e_4 \longleftrightarrow e_2 \longleftrightarrow q_1 \longleftrightarrow e_3 \longleftrightarrow e_5 \tag{8}$$

The case where two qubits are coupled to a one-particle environment ($m = 2$ and $n = 1$) is used to develop an entangling quantum gate (specifically, the controlled-NOT gate) in the presence of a simple environment. This system can be modeled by the following two-dimensional triangular lattice:

$$
\begin{array}{ccc}
 & e_3 & \\
\gamma_{13} \nearrow & & \searrow \gamma_{23} \\
q_1 & \xleftrightarrow{\gamma_{12}} & q_2
\end{array}
\tag{9}
$$

where the two qubits are denoted as q_1 and q_2, and the environmental particle as e_3. Such a model is relevant, for example, for a dilute nuclear spin bath [3]. Values for this set of coupling constants are given in section 6.4.

3. The distance measure

Our objective is to generate an evolution of the QIP which at some time t_f will be as close as possible to the target quantum gate. The problem of evaluating the actual gate fidelity is complicated by the fact that the evolution of the QIP is non-unitary due to the

interaction with the environment. Nevertheless, it is possible to define a useful measure of the distance between the target quantum gate of the QIP and the actual evolution operator of the composite system [41].

Let $U(t) \in \mathrm{U}(2^N)$ be the unitary time-evolution operator of the composite system and $G \in \mathrm{U}(2^m)$ be the unitary target transformation for the quantum gate of the QIP (where $\mathrm{U}(d)$ denotes the group of all $d \times d$ unitary matrices). The evolution of the composite system is governed by the Schrödinger equation,

$$\dot{U}(t) = -\mathrm{i}H(t)U(t), \tag{10}$$

with the initial condition $U(0) = I_{2^N}$ (where I_d denotes the $d \times d$ identity matrix). The gate fidelity depends on the distance between the actual evolution $U \equiv U(t_\mathrm{f})$ at the final time t_f and the target transformation G. In order to perform a perfect gate, it suffices for the time-evolution operator at $t = t_\mathrm{f}$ to be in a tensor-product form $U_\mathrm{opt} = G \otimes \Phi$, where $\Phi \in \mathrm{U}(2^n)$ is an arbitrary unitary transformation acting on the environment.‡ Therefore, the following objective functional is proposed [41] as the measure of the distance between U and G:

$$J = \lambda_N \min_{\Phi} \left\{ \|U - G \otimes \Phi\| \mid \Phi \in \mathrm{U}(2^n) \right\}, \tag{11}$$

where $\| \cdot \|$ is a matrix norm on the space $M_d(\mathbb{C})$ of $d \times d$ complex matrices (in the present case $d = 2^N$), λ_N is a normalization factor, and J is minimized over the set of all unitary Φ. It is useful to expand G, Φ, and U in orthonormal bases. Let $\{|i\rangle\}$, $\{|\nu\rangle\}$ and $\{|i\rangle \otimes |\nu\rangle\}$ be orthonormal bases that span the Hilbert spaces of the QIP, environment, and composite system, respectively. The corresponding expansions read

$$G = \sum_{i,i'=1}^{2^m} G_{ii'}|i\rangle\langle i'|, \quad \Phi = \sum_{\nu,\nu'=1}^{2^n} \Phi_{\nu\nu'}|\nu\rangle\langle\nu'|, \tag{12a}$$

$$U = \sum_{i,i'=1}^{2^m} \sum_{\nu,\nu'=1}^{2^n} U_{\substack{ii' \\ \nu\nu'}} |i\rangle\langle i'| \otimes |\nu\rangle\langle\nu'|. \tag{12b}$$

Using in (11) the Frobenius norm, defined as

$$\|X\|_\mathrm{Fr} = \left[\mathrm{Tr}\left(X^\dagger X\right) \right]^{1/2} \quad \forall X \in M_d(\mathbb{C}), \tag{13}$$

and $\lambda_N = 2^{-(N+1)/2}$, the distance measure becomes [41]

$$J = \left[1 - 2^{-N} \mathrm{Tr}\left(\sqrt{Q^\dagger Q}\right) \right]^{1/2}, \tag{14}$$

where $Q \in M_{2^n}(\mathbb{C})$ is given by

$$Q = \sum_{\nu,\nu'=1}^{2^n} \left(\sum_{i,i'=1}^{2^m} G_{ii'}^* U_{\substack{ii' \\ \nu\nu'}} \right) |\nu\rangle\langle\nu'|. \tag{15}$$

‡ We do not consider in the present work a more general situation where the composite system itself is open and Φ may not be unitary.

Since $0 \leq J \leq 1$, it is convenient to define the gate fidelity as $F = 1 - J$. An important property of this distance measure is its independence of the initial state. In contrast to some other distance measures,§ J is evaluated directly from the evolution operator U, with no need to specify the initial state of the system. This property of J reflects our objective of generating a specified target transformation for whatever initial state, pure or mixed, direct-product or entangled.

Note that in the ideal case when there is no coupling to the environment, i.e., the QIP is a closed system with unitary dynamics, the distance measure (14) becomes

$$J = \left[1 - 2^{-m} \left| \mathrm{Tr} \left(G^{\dagger} U_{\mathrm{q}} \right) \right| \right]^{1/2},$$ (16)

where $U_{\mathrm{q}} \equiv U_{\mathrm{q}}(t_{\mathrm{f}})$ is the unitary evolution operator of the QIP at the final time. Another distance measure used in the literature [37] for closed systems is $J_{\mathrm{cs}} = 1 - 2^{-m} \left| \mathrm{Tr}(G^{\dagger} U_{\mathrm{q}}) \right|$, i.e., $J_{\mathrm{cs}} = J^2$. For example, in section 6 we report optimization results which, in the case of closed QIP systems, are $J \sim 10^{-6}$ and $J \sim 10^{-4}$ for one- and two-qubit gates, respectively, corresponding to the values $J_{\mathrm{cs}} \sim 10^{-12}$ and $J_{\mathrm{cs}} \sim 10^{-8}$, respectively.

4. Decoherence dynamics of the uncontrolled system

The loss of coherence in the QIP, caused by the interaction with the environment, is detrimental to the quantum gate performance. In order to better understand the mechanism of optimal control, we first study the decoherence process in the uncontrolled system. The state of the QIP at time t is described by the reduced density matrix:

$$\rho_{\mathrm{q}}(t) = \mathrm{Tr}_{\mathrm{env}} \left[\rho(t) \right],$$ (17)

where $\rho(t)$ is the density matrix of the composite system and $\mathrm{Tr}_{\mathrm{env}}$ denotes the trace over the environment. A useful measure of decoherence is the von Neumann entropy [47]:

$$S_{\mathrm{vN}}(t) = -\mathrm{Tr} \left\{ \rho_{\mathrm{q}}(t) \ln \left[\rho_{\mathrm{q}}(t) \right] \right\}.$$ (18)

For a pure state, $S_{\mathrm{vN}} = 0$, while for a maximally mixed state of a k-level system, $S_{\mathrm{vN}} = \ln(k)$. We explore the decoherence dynamics of the QIP by studying the time evolution of the entropy $S_{\mathrm{vN}}(t)$ for the uncontrolled system (in this section) and under the influence of optimal time-dependent control fields (in subsequent sections). The initial state used for the entropy calculations is

$$|\Psi_0\rangle = \bigotimes_{i=1}^{m} |-\rangle_i \otimes \bigotimes_{j=m+1}^{N} |+\rangle_j$$ (19)

(i.e., initially all qubits are in the state $|-\rangle$ and all environmental particles are in the state $|+\rangle$). Recall that the distance measure J of (14) is independent of the initial state

§ Relationships between various distance measures, including some presented in [46] and generalizations of (14), are discussed in more detail in [41].

and consequently so are the optimal control fields found for the target gates and the corresponding fidelities. We choose some initial state only for the entropy calculations, which are done to illustrate the decoherence dynamics *after* the time-evolution operator is determined (for either a controlled or uncontrolled system). Therefore, the specific choice of the initial state (19) places no limitations whatsoever on the generality of the optimal control results.

We set the unit of time, thereby introducing a natural system of units, by arbitrarily choosing $\omega_1 = 1$ for all simulations (this implies that one period of the first qubit's free evolution is 2π). Details of the dynamics depend on the system parameters (i.e., the frequencies and coupling constants for the uncontrolled system). In the simplest case of the uncontrolled system of one qubit coupled to a one-particle environment ($m = n = 1$), the initial state is $|\Psi_0\rangle = |-\rangle_1 \otimes |+\rangle_2$, and the time evolution can be solved analytically:

$$|\Psi(t)\rangle = e^{-i\gamma t/4} \left\{ \cos\left(\Omega t\right) |-+\rangle + i\sin\left(\Omega t\right) \left[\frac{\omega_1 - \omega_2}{2\Omega}|-+\rangle + \frac{\gamma}{2\Omega}|+-\rangle \right] \right\}, \tag{20}$$

$$\rho_q(t) = \cos^2\left(\Omega t\right) |-\rangle\langle-| + \sin^2\left(\Omega t\right) \left[\frac{(\omega_1 - \omega_2)^2}{4\Omega^2}|-\rangle\langle-| + \frac{\gamma^2}{4\Omega^2}|+\rangle\langle+| \right], \tag{21}$$

where we use a simplified notation: $|-+\rangle = |-\rangle_1 \otimes |+\rangle_2$, $|+-\rangle = |+\rangle_1 \otimes |-\rangle_2$, and $\Omega = \frac{1}{2}[(\omega_1 - \omega_2)^2 + \gamma^2]^{1/2}$ is the Rabi frequency. Due to discreteness of the environment's spectrum, the loss of coherence is reversible. If the transition frequencies are degenerate, $\omega_1 = \omega_2$, then the state of the composite system, $|\Psi(t)\rangle$, oscillates between two direct-product states, $|-+\rangle$ and $|+-\rangle$. In this case, complete coherence revivals will occur whenever $\sin(\Omega t) = 0$ or $\cos(\Omega t) = 0$, i.e., at times $t_k^{(\text{deg})} = k\pi/(2\Omega)$ ($k \in \mathbb{N}$). However, if $\omega_1 \neq \omega_2$, then $|\Psi(t)\rangle$ oscillates between the initial direct-product state $|-+\rangle$ and an entangled state (a superposition of $|-+\rangle$ and $|+-\rangle$). Therefore, complete coherence revivals will occur only when $\sin(\Omega t) = 0$, i.e., at times $t_k = k\pi/\Omega$ ($k \in \mathbb{N}$). If $|\omega_1 - \omega_2| \ll \gamma$, then, in addition to the complete revivals at times t_k, partial revivals will occur at times $t_k^{(\text{part})} \approx (k - \frac{1}{2})\pi/\Omega$ ($k \in \mathbb{N}$). The maximum loss of coherence depends on the values of γ and $|\omega_1 - \omega_2|$. For a given value of γ, closer frequencies enhance the interaction between the qubit and environment, causing higher peak values of decoherence (i.e., the entropy) and longer revival times. Figure 1 shows the time-evolution of the entropy for the uncontrolled system of one qubit and a one-particle environment, with $\gamma = 0.02$, $\omega_1 = 1$, and various values of ω_2. The entropy dynamics shown in figure 1, obtained by numerically propagating the Schrödinger equation (10), and are in full agreement with the analytical results above. In particular, we find the first-revival times $t_1 \approx \{50.0, 140.7, 313.2\}$ for $\omega_2 = (\pi - x)^{-1}$ and $t_1 \approx \{43.9, 136.1, 313.2\}$ for $\omega_2 = \pi - x$ with $x = \{2, 2.1, 2.14\}$, respectively. These values fully agree with the analytical formula for t_k obtained above. Also, for $x = 2.14$, the frequency difference $|\omega_1 - \omega_2| \approx 0.00159$ is about one order of magnitude smaller than γ, and, correspondingly, a partial revival is found numerically at $t_1^{(\text{part})} \approx 156.6$, in agreement with the analytical result.

For the optimal control simulations below, the system parameters are chosen to ensure complex dynamics and strong decoherence: values of γ/ω are up to 0.02, which

is significant for QC applications, and the frequencies ω_i are close (but not equal), to enhance the interaction. For one qubit coupled to a one-particle environment $(m = n = 1)$, we choose

$$\omega_1 = 1, \quad \omega_2 = (\pi - 2.14)^{-1} \approx 0.99841. \tag{22}$$

Imposing upper limits on the gate duration $(t_f \leq 60)$ and coupling constant $(\gamma \leq 0.02)$ places the dynamics of the uncontrolled system in the regime where decoherence increases monotonically with time (before the entropy reaches its maximum value of $S_{vN} \approx \ln 2$). This dynamical regime approximates some of the effects that the QIP would experience from a larger environment, in particular, preventing restoration of coherence to the qubit by uncontrolled revivals. Thus, any increase in coherence may be attributed exclusively to the action of the control field.

When selecting the parameters of a multiparticle environment, we apply the same criteria for maximizing decoherence of the uncontrolled system, as described above. Figure 2 illustrates the uncontrolled time-evolution of the entropy for a one qubit coupled to n-particle environments $(n = 2, 4, 6)$, with $\gamma = 0.02$. The frequencies of the qubit and pairs of the environmental particles are given by

$$\omega_1 = 1, \tag{23a}$$

$$\omega_j = (\pi - x_j)^{-1}, \quad \omega_{j+1} = \pi - x_j, \quad j = 2, 4, \ldots, n, \tag{23b}$$

$$x_j = \begin{cases} 2.14, & n = 2, \\ 2.14, 2.1, & n = 4, \\ 2.14, 2.1, 2, & n = 6. \end{cases} \tag{23c}$$

For example, for $n = 4$, the frequencies of the four environmental particles are approximately $\{0.96007, 0.99841, 1.00159, 1.04159\}$.

5. Optimal control algorithms

In the context of optimal control, the objective is to maximize the fidelity of the target quantum gate over a set of time-dependent control fields. The target quantum gates considered in this paper include the Hadamard (H_t), identity (I_2), phase $(\pi/8)$, and controlled-NOT (CNOT) transformations:

$$H_t = \frac{1}{\sqrt{2}} \begin{pmatrix} 1 & 1 \\ 1 & -1 \end{pmatrix}, \quad I_2 = \begin{pmatrix} 1 & 0 \\ 0 & 1 \end{pmatrix}, \quad \frac{\pi}{8} = \begin{pmatrix} 1 & 0 \\ 0 & \exp(i\pi/4) \end{pmatrix}, \tag{24a}$$

$$\text{CNOT} = \begin{pmatrix} 1 & 0 & 0 & 0 \\ 0 & 1 & 0 & 0 \\ 0 & 0 & 0 & 1 \\ 0 & 0 & 1 & 0 \end{pmatrix}. \tag{24b}$$

Collectively, H_t, $\pi/8$, and CNOT constitute a universal set of quantum gates for QC [1]. Identity is included to preserve an arbitrary quantum state during a specified time interval, e.g., while operations are performed on other qubits.

In maximizing the gate fidelity, we employ a combination of two optimization techniques, a genetic algorithm and a gradient algorithm. For a given target gate, the genetic algorithm first locates a parameterized control field that achieves a reasonable value of fidelity (e.g., $F > 0.95$), then the gradient algorithm further improves this result by lifting the parameterization restriction on the field. This section describes the details of these search algorithms.

5.1. Optimization with the genetic algorithm

When the genetic algorithm is used, the gate fidelity F is maximized with respect to a parameterized control field

$$C(t) = f(t) \sum_{i=1}^{m} A_i \cos(\tilde{\omega}_i t + \theta_i), \quad 0 \le t \le t_\mathrm{f}. \tag{25}$$

Here, $f(t)$ is an envelope function incorporating the field's spectral width, t_f is the gate duration, and A_i, $\tilde{\omega}_i$, and θ_i are the amplitude, central angular frequency, and relative phase of the ith component of the field, respectively. A combination of these optimization parameters (called "genes") represents an "individual" whose "fitness" is defined as the fidelity of the gate generated by the corresponding field. A collection of individuals constitutes a "population" (we use population sizes of ~ 250). At each generation, we evaluate the fitness of all population members and create the next generation by crossover and mutation of genes of the fittest individuals (crossover and mutation rates are between 20 and 40 percent). A novelty of this algorithm implementation is the inclusion of the control duration t_f as one of the optimization parameters.

5.2. Optimization with the gradient algorithm

Removing the constraints on the control field imposed by the parameterized form (25) provides the potential for more effective control of the system. In this case optimal control fields are found by minimizing the following functional [34]:

$$K = J + \mathrm{Re} \int_0^{t_\mathrm{f}} \mathrm{Tr} \left\{ \left[\dot{U}(t) + iH(t)U(t) \right] B(t) \right\} \mathrm{d}t + \frac{\alpha}{2} \int_0^{t_\mathrm{f}} |C(t)|^2 \, \mathrm{d}t. \tag{26}$$

In addition to the distance measure J of (14), K includes a constraining term and a cost term. Upon minimization of K, the first integral constrains $U(t)$ to obey the Schrödinger equation ($B(t)$ is an operator Lagrange multiplier) and the second integral term penalizes the field fluence,

$$\mathcal{E} = \int_0^{t_\mathrm{f}} |C(t)|^2 \, \mathrm{d}t, \tag{27}$$

with a weight $\alpha > 0$.

5.2.1. Optimal control equations. An optimal control field is obtained by solving a set of equations that follow from the variational analysis of K as a functional of $B(t)$ and $U(t)$. Here, we derive the corresponding functional derivatives [48] and boundary conditions. The functional derivative of K with respect to $B(t)$ yields

$$\frac{\delta K}{\delta B(t)} = \text{Re}\left\{\left[\dot{U}(t) + iH(t)U(t)\right]^T\right\}, \tag{28}$$

so that the condition $\delta K/\delta B(t) = 0$ results in the Schrödinger equation (10) for $U(t)$. Next we compute the functional derivative of K with respect to $U(t)$:

$$\frac{\delta K}{\delta U(t)} = \text{Re}\left\{\frac{\delta J}{\delta U(t)} + B^T(t_{\text{f}})\delta(t - t_{\text{f}}) - \left[\dot{B}(t) - iB(t)H(t)\right]^T\right\}. \tag{29}$$

Since J depends only on $U = U(t_{\text{f}})$, we obtain $\delta J/\delta U(t) = (\text{d}J/\text{d}U)\delta(t - t_{\text{f}})$. Therefore, the condition $\delta K/\delta U(t) = 0$ results in two equations:

$$\dot{B}(t) = iB(t)H(t), \tag{30}$$

$$B^T(t_{\text{f}}) = -\frac{\text{d}J}{\text{d}U}. \tag{31}$$

We will also use the functional derivative of K with respect to $C(t)$,

$$\frac{\delta K}{\delta C(t)} = \text{Im}\left\{\text{Tr}\left[\hat{\mu}U(t)B(t)\right]\right\} + \alpha C(t), \tag{32a}$$

$$\hat{\mu} = \sum_i^m \mu_i S_{ix}, \tag{32b}$$

to guide the gradient search, as described in section 5.2.2 below.

The initial condition for $U(t)$ is $U(0) = I_{2^N}$ and the final condition for $B(t)$ is given by (31). In order to find the explicit form of $\text{d}J/\text{d}U$, first consider a scalar function $y(Z(x))$, where Z is a matrix function of the scalar variable x. Using the chain rule, we obtain

$$\frac{\text{d}y}{\text{d}x} = \sum_{\kappa,\kappa'} \frac{\text{d}y}{\text{d}Z_{\kappa\kappa'}} \frac{\text{d}Z_{\kappa\kappa'}}{\text{d}x} = \sum_{\kappa,\kappa'} \frac{\text{d}y}{\text{d}Z_{\kappa\kappa'}} \frac{\text{d}Z^T_{\kappa'\kappa}}{\text{d}x} = \text{Tr}\left(\frac{\text{d}y}{\text{d}Z} \frac{\text{d}Z^T}{\text{d}x}\right). \tag{33}$$

Setting $y = \text{Tr}(Z)$, implies that

$$\frac{\text{d}y}{\text{d}Z} = I. \tag{34}$$

Now let $Z = \left(Q^\dagger Q\right)^{1/2}$ and $x = U_{ab}$ (a complex scalar variable). The matrix indices a and b range from 1 to 2^N. Note that $\left(Q^\dagger Q\right)^{1/2}$ is not an analytic function of U_{ab}, but it can be expressed as an analytic function of U_{ab} and U^*_{ab}. Therefore, a generalized complex derivative [48] is applied to calculate $\text{d}Z/\text{d}x$, so that U^*_{ab} and subsequently $Q^\dagger$ are treated as constants when differentiating $\left(Q^\dagger Q\right)^{1/2}$ with respect to U_{ab}. Thus we find that

$$\frac{\text{d}Z}{\text{d}x} = \frac{\text{d}\left(Q^\dagger Q\right)^{1/2}}{\text{d}U_{ab}} = \frac{1}{2}\left(Q^\dagger Q\right)^{-1/2} Q^\dagger \frac{\text{d}Q}{\text{d}U_{ab}}. \tag{35}$$

By combining (33)-(35), we obtain

$$\frac{\mathrm{d}y}{\mathrm{d}x} = \frac{\mathrm{d}}{\mathrm{d}U_{ab}} \mathrm{Tr}\left[(Q^\dagger Q)^{1/2}\right] = \frac{1}{2}\mathrm{Tr}\left[(Q^\dagger Q)^{-1/2} Q^\dagger \frac{\mathrm{d}Q}{\mathrm{d}U_{ab}}\right]. \tag{36}$$

With the above notation, $J = (1 - 2^{-N}y)^{1/2}$. Noting that $(\mathrm{d}J/\mathrm{d}U)_{ab} = \mathrm{d}J/\mathrm{d}U_{ab}$ and using (36), we finally derive

$$\left(\frac{\mathrm{d}J}{\mathrm{d}U}\right)_{ab} = -\frac{2^{-N}}{4}\left\{1 - 2^{-N}\mathrm{Tr}\left[(Q^\dagger Q)^{1/2}\right]\right\}^{-1/2}\mathrm{Tr}\left[(Q^\dagger Q)^{-1/2} Q^\dagger \frac{\mathrm{d}Q}{\mathrm{d}U_{ab}}\right], \tag{37a}$$

$$\frac{\mathrm{d}Q}{\mathrm{d}U_{ab}} = G^*_{\lceil a/2^n \rceil \lceil b/2^n \rceil}|a \bmod 2^n\rangle\langle b \bmod 2^n|. \tag{37b}$$

Equation (37b) is obtained from (15), using the fact that $k \bmod k = k$. In (37b), the states are elements of the environment's orthonormal basis $\{|\nu\rangle\}$, and $\lceil x \rceil$ denotes the smallest integer greater than or equal to x. The explicit form of the boundary condition for $B(t)$ is obtained by substituting (37) into (31).

5.2.2. The numerical procedure. Optimal control fields are found using an iterative gradient algorithm described below. An initial guess for the control field is needed at the first iteration. Typically, we use the output of the genetic algorithm as the initial guess for faster convergence, although fields of the form (25) with a random choice of parameters can be used as well. At each iteration, $U(t)$ is propagating forward in time with the Schrödinger equation (10) and the initial condition $U(0) = I_{2^N}$. The resulting matrix $U = U(t_\mathrm{f})$ is used to determine the final condition (31) for $B(t_\mathrm{f})$. Then $B(t)$ is propagated backward in time with the time-reversed Schrödinger equation (30). All propagations are performed using a toolkit for computational efficiency [49]. The resulting $U(t)$ and $B(t)$ are utilized to compute the functional derivative $\delta K/\delta C(t)$ of (32), which then adjusts the control field for the next iteration. The adjustment of the control field for the kth iteration ($k \in \mathbb{N}$) is given by

$$C^{(k)}(t) = C^{(k-1)}(t) - \beta\sin^r(\pi t/t_\mathrm{f}) \left.\frac{\delta K}{\delta C(t)}\right|_{C(t)=C^{(k-1)}(t)}, \tag{38}$$

where $0 < \beta \leq 1$ and $\frac{1}{2} \leq r \leq 1$ are constants used to modify the magnitude of the field adjustment. The multiplier $\sin^r(\pi t/t_\mathrm{f})$ ensures that the control field $C(t)$ is nearly zero at the initial and final time, which is a reasonable physical restriction on the field. This iteration routine continues until we observe no further improvement in K, which manifests the achievement of convergence.

Despite the lack of direct coupling of the control field to the environment, it can be shown that the composite system described by (1) is completely controllable (up to a global phase), as defined in [50]. However, the restrictions on the gate duration and on the shape of the control field limit the achievable fidelity.

6. Results of optimal control in the presence of decoherence

6.1. One qubit coupled to a one-particle environment

We consider the optimally controlled Hadamard, identity, and phase gates generated for a single qubit coupled to a one-particle environment ($m = n = 1$). Fidelities for these one-qubit gates are presented in figure 3 for various values of the coupling constant γ. The control fields optimized for the actual values of γ result in fidelities above 0.9991. In particular, for the Hadamard transform, we obtain $F > 1 - 10^{-6}$ for $\gamma = 0$ (a closed system) and $F \approx 0.9995$ for $\gamma = 0.02$ (the strongest coupling considered). In contrast, when the control field optimized for $\gamma = 0$ is applied to the system with $\gamma = 0.02$, it generates a gate with a poor fidelity, $F \approx 0.9063$. This result demonstrates that optimal solutions designed for the ideal case of a closed system have little value when applied to realistic open systems. However, the optimal control algorithm is able to generate quantum gates with very high fidelities, if coupling to the environment is explicitly taken into account.

The optimal control fields that generate the one-qubit gates (with a one-particle environment and $\gamma = 0.02$) are shown in figure 4. These fields are intense, with maximum amplitudes larger than 2.0 (in the units of $\hbar = \omega_1 = \mu_i = 1$). The gate duration is $t_\mathrm{f} = 25.0$ (about four periods of free evolution). The exact time structure of an optimal field is not intuitive and is tailored to the particular control application. For example, control fields optimized for $\gamma = 0.02$ are not only more intense than those optimized for $\gamma = 0$, they also have very different structures. One common feature of the optimal control fields presented in figure 4 is that they are approximately symmetric about $t \approx t_\mathrm{f}/2$. We suggest that this property of the fields is related to the reversibility of the system dynamics: the periods in which the information flows from the QIP to the environment are followed by periods in which the information flow is reversed, in order to restore the coherence of the QIP.

Figure 5 shows the time behavior of the von Neumann entropy of the QIP for optimally controlled one-qubit gates (with $t_\mathrm{f} = 25.0$ and $\gamma = 0.02$). By comparing figures 5 and 1, we observe that the optimal control dramatically enhances coherence of the qubit system in comparison to the uncontrolled dynamics. Decoherence is suppressed by the control at all times, but especially at the end of the gate operation (i.e., for $t = t_\mathrm{f}$). For example, $S_\mathrm{vN}(t_\mathrm{f}) < 10^{-7}$ for the Hadamard gate with $\gamma = 0.02$, which means that at $t = t_\mathrm{f}$ the qubit system and environment are almost completely uncoupled. Inspecting eigenvalues of the controlled Hamiltonian, we find that the intense control field creates significant dynamic shifts of the energy levels. Specifically, under the influence of the optimal control field, four of the six transition frequencies of the composite system experience high-amplitude oscillations (following the corresponding changes in the field strength). This effect is mainly responsible for reducing the qubit-environment interaction during the control pulse. However, achieving extremely low final-time entropies and correspondingly high gate fidelities requires the employment of an induced coherence revival. For the selected set of the system parameters, revivals in

the uncontrolled dynamics occur at times much longer than $t_{\rm f}$ (specifically, $t_1^{\rm (part)} \approx 156.6$ and $t_1 \approx 313.2$), so that the almost complete coherence revival observed at $t = t_{\rm f}$ is induced exclusively by the control field.

For very short gate durations ($t_{\rm f} < 5$), a different type of optimal solution is found. The control fails to induce revivals at such short times and therefore generates gates with smaller fidelities (e.g., $F \approx 0.9874$ for the Hadamard transform with $\gamma = 0.02$ and $t_{\rm f} \approx 2.33$). In this short-time regime the control relies on the decoherence suppression via dynamic shifting of the energy levels and on very fast operation (trying to perform the target transformation in the shortest time possible to limit the effect of decoherence), but not on the creation of coherence revivals. Such short-time controls can be useful for environments with very dense spectra, for which the induced-revival times will be impractically long.

We study in detail how the choice of the control duration $t_{\rm f}$ affects properties of the optimal control field, gate fidelity, and decoherence dynamics. Specifically, we optimize the one-qubit Hadamard gate (with a one-particle environment and $\gamma = 0.02$) for all integer values of $t_{\rm f}$ between 2 and 40 using the gradient algorithm described in section 5.2. For $t_{\rm f} < 5$ we find the fast-control no-revival regime described above. Interestingly, most optimal control fields with $t_{\rm f} > 5$, in addition to inducing an almost complete coherence revival at the final time, also produce a partial revival at approximately $t_{\rm f}/2$. Optimal control fields with $5 < t_{\rm f} < 20$ typically exhibit large amplitudes and fluences and strong low-frequency components. For $t_{\rm f} = 25$ we find the optimal control field that generates the quantum gate with a better fidelity while having a smaller amplitude and fluence, as compared to the fields obtained for shorter control durations. As $t_{\rm f}$ increases to 25, the gate fidelity increases to approximately 0.9995, the final-time entropy decreases to approximately 10^{-7}, and the maximum field amplitude decreases to approximately 2.0. However, increasing $t_{\rm f}$ above 25 does not improve the optimal gate performance; the field amplitudes, gate fidelities, and final-time entropy values change very slightly for $25 \le t_{\rm f} \le 40$. The physical interpretation of this behavior is that the control requires some time ($t_{\rm f} \ge 25$ in the present case) to almost completely reverse the information flow between the QIP and environment, and induce a nearly perfect coherence revival. From these results, it appears that the pulse duration is a very important characteristic of the control fields employed for quantum gate generation.

6.2. The Kraus-map dynamics of the qubit

The time-dependent state of the QIP, which is coupled to the environment, is represented by the reduced density matrix (17). In order to examine the reduced dynamics of the QIP, it is instructive to use the Kraus-map representation [51]. If the composite system was initially (i.e., at time $t = 0$) in the direct-product state,

$$\rho(0) = \rho_{\rm q}(0) \otimes \rho_{\rm env}(0) = \rho_{\rm q}(0) \otimes \sum_{\nu=1}^{2^n} \varrho_\nu |\nu\rangle\langle\nu|, \tag{39}$$

then the reduced dynamics of the QIP has the following form (known as the Kraus map [51]):

$$\rho_{\mathrm{q}}(t) = \Phi[\rho_{\mathrm{q}}(0)] = \sum_{\nu,\nu'=1}^{2^n} K_{\nu\nu'}(t)\rho_{\mathrm{q}}(0)K_{\nu\nu'}^{\dagger}(t), \tag{40}$$

where the Kraus operators $K_{\nu\nu'}(t) \in M_{2^m}(\mathbb{C})$ are given by

$$K_{\nu\nu'}(t) = \sqrt{\varrho_{\nu'}} \sum_{i,i'=1}^{2^m} U_{ii'\atop \nu\nu'}(t)|i\rangle\langle i'|, \tag{41a}$$

$$\sum_{\nu,\nu'=1}^{2^n} K_{\nu\nu'}^{\dagger}(t)K_{\nu\nu'}(t) = I_{2^m}. \tag{41b}$$

It is well known [51] that there exist infinitely many different sets of Kraus operators, $\{K_1,\ldots,K_p\}$ (where $p \in \mathbb{N}$ is the number of operators in the set), that represent the same map Φ (i.e., they evolve $\rho_{\mathrm{q}}(0)$ in exactly the same way). Moreover, any Kraus map for an k-level quantum system can be represented by a set of $p \leq k^2$ Kraus operators. That is, if the map is represented by a set of $p' > k^2$ Kraus operators, there always exists another representation with not more than k^2 operators. Therefore, for our system of m qubits and n environmental particles, the set of 2^{2n} Kraus operators (41a) can always be transformed into another set of not more than 2^{2m} operators, representing the same map Φ. However, since we numerically study Kraus operators only for the case of $n = m = 1$, there is no practical need for such a transformation.

In calculations, we use $\rho(0) = |\Psi_0\rangle\langle\Psi_0|$ with $|\Psi_0\rangle$ of (19). For one qubit coupled to a one-particle environment, we use the notation $|\nu = 1\rangle = |+\rangle$ and $|\nu = 2\rangle = |-\rangle$ and find $K_{12}(t) = K_{22}(t) = 0$ and $K_{11}^{\dagger}(t)K_{11}(t) + K_{21}^{\dagger}(t)K_{21}(t) = I_2$. It is therefore sufficient to explore either $K_{11}(t)$ or $K_{21}(t)$. By evaluating the Kraus operators we can quantify the non-unitarity of the qubit dynamics. It is important to note that the non-unitary evolution is not only responsible for decoherence, but is also required to steer the information flow back to the QIP. The control field that restores coherence to the QIP necessarily employs the interaction with the environment and the corresponding non-unitary dynamics. We examine the time behavior of the Frobenius norm of the Kraus operator, $\|K_{21}(t)\|_{\mathrm{Fr}}$, that serves as a measure of non-unitarity. Figure 6 shows $\|K_{21}(t)\|_{\mathrm{Fr}}$ for both controlled and uncontrolled dynamics. In comparison to the uncontrolled evolution, the optimal control dramatically decreases the non-unitarity of the qubit dynamics during the gate operation, culminating in almost complete decoupling at the final time t_{f}. We also see that, under the optimal control, $\|K_{21}(t)\|_{\mathrm{Fr}}$ is approximately symmetric about $t \approx t_{\mathrm{f}}/2$. Inspecting the time derivative of the entropy, $\mathrm{d}S_{\mathrm{vN}}/\mathrm{d}t$, we find that $\|K_{21}(t)\|_{\mathrm{Fr}}$ reaches the maximum at approximately the same time (just prior to $t_{\mathrm{f}}/2$) when the fastest decrease in the qubit's entropy is observed, indicating the maximum flow of information into the QIP.

Table 1. The performance of the optimally controlled one-qubit Hadamard gate in the presence of various n-particle environments ($\gamma = 0.02$). Here, $A_{\max}$, t_{f}, $\mathcal{E}$, F, and $S_{\mathrm{vN}}(t_{\mathrm{f}})$ are the maximum field amplitude, control duration, field fluence, gate fidelity, and final-time entropy, respectively. $F_{\gamma=0}$ denotes the gate fidelity obtained when the control field optimized for $\gamma = 0$ is applied to the system with $\gamma = 0.02$. The initial state for the entropy computation is $|\Psi_0\rangle$ of (19).

n	1	2	4	6
$A_{\max}$	2.0	4.0	4.0	2.5
t_{f}	25.0	15.4	25.0	25.0
$\mathcal{E}$	20.0	49.0	55.5	34.0
F	0.9995	0.9975	0.9935	0.9786
$F_{\gamma=0}$	0.9063	0.8829	0.8133	0.7723
$S_{\mathrm{vN}}(t_{\mathrm{f}})$	9.0×10^{-8}	4.4×10^{-5}	4.7×10^{-4}	3.0×10^{-3}

6.3. One qubit coupled to a multiparticle environment

We explore the performance of optimally controlled one-qubit gates in the presence of multiparticle environments described in section 2. Table 1 reports optimal control field parameters, fidelity, and final-time entropy for the one-qubit Hadamard gate coupled to n-particle environments ($m = 1$, $n = 1, 2, 4, 6$, and $\gamma = 0.02$). For $n = 4$, the values in Table 1 were obtained with the coupling scheme modeled by a two-dimensional lattice of (7); however, very similar results were obtained with the linear nearest-neighbor coupling scheme of (8).

The results obtained for $n \geq 2$ further illustrate the benefits of optimal controls which explicitly take into account coupling to the environment. The entropy dynamics indicate that for multiparticle environments the control employs the same mechanism of an induced coherence revival, as described above for $n = 1$. Fast and intense control fields significantly suppress the qubit-environment interaction during the gate operation and try to recover as much of the lost information as possible before the end of the control pulse. However, as the complexity of the composite system increases, it becomes more difficult to induce an almost perfect revival; therefore, the gate fidelity and final-time coherence decrease as n increases. This observation supports the conclusion that shorter-time controls (which do not rely on revivals) will be useful for environments with dense spectra.

6.4. Two qubits with a one-particle environment

For the QIP consisting of two qubits ($m = 2$), the target gate is CNOT of (24b). The coupling constant between the two qubits is $\gamma_{12} = 0.1$, while the coupling constant between each qubit and the single environmental particle ($n = 1$) is $\gamma_{13} = \gamma_{23} = \gamma$. Frequencies of the two qubits are $\omega_1 = 1$ and $\omega_2 = \pi - 2.05 \approx 1.09519$, and the frequency of the environmental particle is $\omega_3 = (\pi - 2.14)^{-1} \approx 0.99841$. The optimal control fields obtained for $\gamma = 0$ and $\gamma = 0.01$ (shown in figure 7) generate the CNOT

gate with fidelities of 0.9999 and 0.9798, respectively. When $\gamma = 0.01$, the entropy for the uncontrolled evolution increases monotonically until $t \approx 125$ (reaching a maximum of approximately 0.6), whereas the optimal control field results in a much lower entropy, shown in sub-plot (b) of figure 8. The same pattern of a partial revival at an intermediate time followed by an almost complete revival at $t = t_\mathrm{f}$, seen for the one-qubit gates in figure 5, is also present for the two-qubit gate, but on a longer time scale. For the CNOT gate's final-time coherence revival we find $S_\mathrm{vN}(t_\mathrm{f}) \approx 1.5 \times 10^{-3}$ at $t_\mathrm{f} = 121.1$.

We observe that the fidelity of the optimally controlled quantum gates decreases with increases in n (the number of environmental particles) and, even more significantly, m (the number of qubits in the QIP). This behavior arises due to the difference between the perfect control solution and an actual control field found by the optimization algorithm. According to an analysis of the control landscape for unitary transformations [52, 53], the pernicious effect of control inaccuracies on the gate fidelity rapidly increases with the size of the system. If instead of the perfect control solution $C_0(t)$, the actual field is $C_0(t) + \delta C(t)$, then instead of the perfect fidelity $F = 1$, one will obtain $F = 1 - \delta F$, where $\delta F \propto 2^m \|\delta C(t)\|^2$ (here, $\| \cdot \|$ denotes an appropriate functional norm). As the number of interacting qubits, m, increases, the factor 2^m becomes more important. Moreover, as the complexity of the composite system increases (more qubits and/or environmental particles), the control error $\|\delta C(t)\|$ will increase as well, as it will become more difficult to find a field that is very close to the perfect one.

6.5. Can the state purity measure the gate fidelity?

We found that obtaining a very high gate fidelity requires an almost complete coherence revival characterized by a very low final-time entropy. Is it then possible to rely on a characteristic of coherence (e.g., the final-time entropy or purity of the QIP state) as a measure of the gate quality, instead of measuring the distance between the actual and target gate transformations? The answer is definitely "no" because the restoration of coherence is a necessary, but not sufficient, condition for a high gate fidelity. There exist an infinite number of unitary, or almost unitary, transformations which nevertheless are very far from the target one.

In order to further emphasize this point, we generalize the notion of the gate fidelity (as measured by the distance between the actual evolution operator $U(t)$ and target transformation G) to all times $0 \leq t \leq t_\mathrm{f}$. Figure 8 shows this time-dependent fidelity $F(t)$ and the entropy $S_\mathrm{vN}(t)$ for the optimally controlled two-qubit CNOT gate (with $\gamma = 0.01$ and $t_\mathrm{f} = 121.1$). We see that the minimum of the entropy occurs at a time $t_{S_\mathrm{min}} \approx 119$ (i.e., before t_f) when $F(t)$ is still quite low, and that at the time interval between t_{S_min} and t_f, while the fidelity $F(t)$ rapidly increases to achieve its final-time value $F \approx 0.9798$, the entropy slightly increases as well. This example shows that fidelity and coherence do not always correlate and that a very low value of the entropy does not always result in a correspondingly high value of the gate fidelity. According to this analysis, a strategy of maximizing the state purity [38, 40] does not ensure the

generation of target quantum gates with the highest possible fidelity.

7. Robustness of optimally controlled gates to system variations

We observed that applying the control field optimized for the closed system ($\gamma = 0$) to the coupled one ($\gamma = 0.02$) results in a significant decrease in the gate fidelity. Analogously, we find that applying the control field optimized for the case of a one-particle environment ($n = 1$) to systems with $n \geq 2$ environmental particles also has a strong detrimental effect on the gate fidelity. These results are part of a broader analysis of the robustness of optimally controlled quantum gates to different types of system variations.

We address some aspects of this issue by considering the one-qubit Hadamard gate, with a fixed number n of environmental particles ($n = 1, 2, 4$), and finding an optimal control field for a specified set of system parameters: the coupling constants γ_{ij} given by (5) (with $\gamma = 0.02$) and frequencies ω_i given by (22) for $n = 1$ and (23) for $n \geq 2$. Then we apply this control field to an ensemble of systems with normal variations in either coupling constants γ_{ij} or frequencies ω_i and analyze how the uncertainties in the system parameters affect the gate fidelity F and final-time entropy $S_{\text{vN}}(t_{\text{f}})$. Although the dependence of F and $S_{\text{vN}}(t_{\text{f}})$ on the coupling constants and frequencies is highly non-linear (which implies that the distributions of F and $S_{\text{vN}}(t_{\text{f}})$ will not be normal), our statistical analysis employs only mean values and standard deviations, given by $\overline{F} = L^{-1} \sum_{r=1}^{L} F_r$ and $\sigma_F = [L^{-1} \sum_{r=1}^{L} (F_r - \overline{F})^2]^{1/2}$, respectively, for the gate fidelity F, and similarly for the final-time entropy $S_{\text{vN}}(t_{\text{f}})$. The summation is over all elements of the ensemble (ensemble sizes L of the order of 10^5 are used in the calculations).

7.1. Variation of the coupling constants

The value of each non-zero coupling constant γ_{ij} (given by (5) with $\gamma = 0.02$) is individually replaced by a value randomly selected from a normal distribution with a mean $\overline{\gamma} = 0.02$ and a standard deviation $\sigma_\gamma = \overline{\gamma}/8 = 0.0025$. The statistical analysis of the corresponding distributions of the fidelity and final-time entropy is reported in table 2, and frequency histograms of these distributions are shown in figure 9. These results demonstrate a high degree of robustness of the performance of the optimally controlled gate to relatively large variations in the strength of the system-environment coupling. On average, there is practically no decrease in the fidelity and entropy, and the relative width of the fidelity distribution, $\sigma_F/\overline{F}$, is by several orders of magnitude smaller than $\sigma_\gamma/\overline{\gamma}$. Interestingly, if the control field optimized for $\gamma = 0.02$ is applied to the closed system with $\gamma = 0$, this results in a relatively high fidelity (e.g., $F = 0.9989$ for $n = 1$). The standard deviation σ_F rises with the increase in the number of environmental particles. We also see that the distributions of F and $S_{\text{vN}}(t_{\text{f}})$ are more symmetric for $n = 4$ than for $n = 1$.

Table 2. Fidelity and entropy data for the one-qubit Hadamard gate applied to an ensemble of systems with normal variations in the coupling constants γ_{ij} and frequencies ω_i. Columns of F and $S_{\text{vN}}(t_{\text{f}})$ contain fidelity and final-time entropy values, respectively, for the original system parameters: $\gamma = 0.02$ and frequencies given by (22) for $n = 1$ and (23) for $n \geq 2$. Columns of $\overline{F}$ and $\overline{S_{\text{vN}}}$ contain mean values of fidelity and final-time entropy, respectively, over the ensemble, while σ_F and $\sigma_{S_{\text{vN}}}$ are the respective standard deviations.

			Variation in γ_{ij}			
n	F	$\overline{F}$	σ_F	$S_{\text{vN}}(t_{\text{f}})$	$\overline{S_{\text{vN}}}$	$\sigma_{S_{\text{vN}}}$
1	0.9995	0.9995	1.1×10^{-4}	9.0×10^{-8}	1.0×10^{-7}	4.7×10^{-8}
2	0.9975	0.9975	2.6×10^{-4}	4.4×10^{-5}	4.6×10^{-5}	1.5×10^{-5}
4	0.9935	0.9934	6.1×10^{-4}	4.7×10^{-4}	4.8×10^{-4}	8.1×10^{-5}
			Variation in ω_i			
n	F	$\overline{F}$	σ_F	$S_{\text{vN}}(t_{\text{f}})$	$\overline{S_{\text{vN}}}$	$\sigma_{S_{\text{vN}}}$
1	0.9995	0.9821	1.1×10^{-2}	9.0×10^{-8}	6.8×10^{-3}	7.4×10^{-3}
2	0.9975	0.9896	5.3×10^{-3}	4.4×10^{-5}	7.0×10^{-4}	6.2×10^{-4}
4	0.9935	0.9884	4.5×10^{-3}	4.7×10^{-4}	1.7×10^{-3}	1.8×10^{-3}

7.2. Variation of the frequencies

The value of each frequency ω_i (given by (22) for $n = 1$ and (23) for $n \geq 2$) is individually replaced by a value randomly selected from a normal distribution with a mean $\overline{\omega}_i = \omega_i$ and a standard deviation $\sigma_{\omega_i} = \omega_i/25$. The statistical analysis of the corresponding distributions of the fidelity and final-time entropy is reported in table 2, and frequency histograms of these distributions are shown in figure 10. It is well known [29, 30, 32] that a high degree of quantum control may be achieved through the complex interference of evolution pathways. This interference strongly depends on the relative phases of all pathways, and these phases in turn depend on the transition frequencies of the system. Therefore, we would expect the optimal gate performance to be much more sensitive to variations in the frequencies than to changes in the coupling constants. The results presented in table 2 and figure 10 corroborate this expectation. Still, the robustness of the optimal gate performance to frequency fluctuations is tolerable. Moreover, the degree of robustness for systems with two and more environmental particles ($n \geq 2$) is even higher than for $n = 1$.

8. Conclusions

This work demonstrates the importance of OCT in designing quantum gates for use in QC, especially in the presence of a decohering environment. The model studied here represents a realistic system of interacting qubits and is relevant for various physical implementations of QC. High quality optimal solutions obtained in the presence of unwanted couplings also exhibit a significant degree of robustness to random variations in the system parameters. The analysis of the system dynamics reveals control

mechanisms which employ fast and intense time-dependent fields to effectively suppress the qubit-environment interaction via dynamic shifting of the energy levels and achieve an almost full coherence recovery via an induced revival.

The results reported in this paper further support the use in QC applications of laboratory closed-loop optimal controls employing learning algorithms and intense ultrafast fields [29, 30]. In the area of molecular dynamics, the utility of optimal control methods was first demonstrated theoretically in very simple model systems; nevertheless, these methods were later applied with great success in the laboratory to complex molecules [29]. Similarly, we expect that the optimal control of quantum gates, the usefulness of which was demonstrated here for a relatively simple environment model, will be also effective for real quantum information systems. A successful application of optimal control methods to the generation of high-fidelity quantum gates in the laboratory will be an important step towards achieving error thresholds required for fault tolerant QC [6, 7].

This work may be further advanced with the use of the control-mechanism analysis [54] to explore the detailed dynamics of the decoherence management process in optimally controlled quantum gates. Methods of landscape analysis [52, 53, 55] may be employed to investigate how optimal controls are deduced and study the effects of control errors in the context of non-unitary dynamics of open quantum systems.

Acknowledgments

References

[1] Nielsen M A and Chuang I L 2000 *Quantum Computation and Quantum Information* (Cambridge: Cambridge University Press)
[2] Loss D and DiVincenzo D P 1998 *Phys. Rev.* A **57** 120
 Burkard G, Loss D and DiVincenzo D P 1999 *Phys. Rev.* B **59** 2070
[3] Kane B E 1998 *Nature* **393** 133
[4] Vrijen R, Yablonovitch E, Wang K, Jiang H W, Balandin A, Roychowdhury V, Mor T and DiVincenzo D 2000 *Phys. Rev.* A **62** 012306
[5] Petta J R, Johnson A C, Taylor J M, Laird E A, Yacoby A, Lukin M D, Marcus C M, Hanson M P and Gossard A C 2005 *Science* **309** 2180
[6] Shor P W 1996 *Proc. 35th Ann. Symp. on Fundamentals of Computer Science* (Los Alamitos: IEEE Press) p 56 (*Preprint* quant-ph/9605011)
[7] Preskill J 1998 *Proc. R. Soc. London, Ser. A* **454** 385
 Knill E, Laflamme R and Zurek W H 1998 *Science* **279** 342
 Aharonov D and Ben-Or M 1999 Fault-tolerant quantum computation with constant error rate *Preprint* quant-ph/9906129
 Steane A M 2003 *Phys. Rev.* A **68** 042322

Knill E 2005 *Nature* **434** 39

[8] Palma G M, Suominen K A and Ekert A K, 1996 *Proc. R. Soc. London, Ser. A* **452** 567

[9] Duan L M and Guo G C 1997 *Phys. Rev. Lett.* **79** 1953

[10] Zanardi P and Rasetti M 1997 *Phys. Rev. Lett.* **79** 3306

[11] Lidar D A, Chuang I L and Whaley K B 1998 *Phys. Rev. Lett.* **81** 2594

Kempe J, Bacon D, Lidar D A and Whaley K B 2001 *Phys. Rev. A* **63** 042307

Lidar D A and Whaley K B 2003 *Irreversible Quantum Dynamics* (*Lecture Notes in Physics* vol 622) ed F Benatti and R Floreanini (Berlin: Springer) p 83

[12] Knill E, Laflamme R and Viola L 2000 *Phys. Rev. Lett.* **84** 2525

[13] Viola L and Lloyd S 1998 *Phys. Rev. A* **58** 2733

Viola L, Knill E and Lloyd S 1999 *Phys. Rev. Lett.* **82** 2417

Viola L, Knill E and Lloyd S 1999 *Phys. Rev. Lett.* **83** 4888

Viola L, Knill E and Lloyd S 2000 *Phys. Rev. Lett.* **85** 3520

[14] Zanardi P 1999 *Phys. Lett. A* **258** 77

[15] Vitali D and Tombesi P 1999 *Phys. Rev. A* **59** 4178

Vitali D and Tombesi P 2001 *Phys. Rev. A* **65** 012305

[16] C. Uchiyama and M. Aihara 2002 *Phys. Rev. A* **66** 032313

[17] Wu L A and Lidar D A 2002 *Phys. Rev. Lett.* **88** 207902

Byrd M S and Lidar D A 2002 *Quantum Inf. Process.* **1** 19

Byrd M S and Lidar D A 2003 *Phys. Rev. A* **67** 012324

[18] Kofman A G and Kurizki G 2004 *Phys. Rev. Lett.* **93** 130406

[19] Facchi P, Tasaki S, Pascazio S, Nakazato H, Tokuse A and Lidar D A 2005 *Phys. Rev. A* **71** 022302

[20] Fanchini F F, Hornos J E M and Napolitano R d J 2006 Protecting quantum logic operations by continuous application of external fields *Preprint* quant-ph/0611188

[21] Mancini S and Bonifacio R 2001 *Phys. Rev. A* **64** 042111

Mancini S, Vitali D, Tombesi P and Bonifacio R 2002 *Europhys. Lett.* **60** 498

Mancini S, Vitali D, Tombesi P and Bonifacio R 2002 *J. Opt. B: Quantum Semiclass. Opt.* **4** S300

[22] Brif C, Rabitz H, Wallentowitz S and Walmsley I A 2001 *Phys. Rev. A* **63** 063404

[23] Zhu W and Rabitz H 2003 *J. Chem. Phys.* **118** 6751

[24] Hohenester U and Stadler G 2004 *Phys. Rev. Lett.* **92** 196801

[25] Sklarz S E, Tannor D J and Khaneja N 2004 *Phys. Rev. A* **69** 053408

[26] Grigorenko I A and Khveshchenko D V 2005 *Phys. Rev. Lett.* **94** 040506

[27] Jirari H and Pötz W 2005 *Phys. Rev. A* **72** 013409

Jirari H and Pötz W 2006 *Phys. Rev. A* **74** 022306

Wenin M and Pötz W 2006 *Phys. Rev. A* **74** 022319

[28] Grace M, Brif C, Rabitz H, Walmsley I, Kosut R and Lidar D 2006 *New J. Phys.* **8** 35

[29] Rabitz H, de Vivie-Riedle R, Motzkus M and Kompa K 2000 *Science* **288** 824 (2000)

[30] Walmsley I and Rabitz H 2003 *Phys. Today* **56** 43

[31] Peirce A P, Dahleh M A and Rabitz H 1988 *Phys. Rev. A* **37** 4950

Dahleh M, Peirce A P and Rabitz H 1990 *Phys. Rev. A* **42** 1065

[32] Warren W, Rabitz H and Dahleh M 1993 *Science* **259** 1581

[33] Sanders G D, Kim K W and Holton W C 1999 *Phys. Rev. A* **59**, 1098

[34] Palao J P and Kosloff R 2002 *Phys. Rev. Lett.* **89** 188301

Palao J P and Kosloff R 2003 *Phys. Rev. A* **68** 062308

[35] Sklarz S E and Tannor D J 2004 Local control theory for unitary transformations: Application to quantum computing without leakage *Preprint* quant-ph/0404081

Sklarz S E and Tannor D J 2006 *Chem. Phys.* **322**, 87

[36] Khaneja N, Reiss T, Kehlet C, Schulte-Herbrüggen T and Glaser S J, 2005 *J. Mag. Res.* **172** 296

[37] Spörl A, Schulte-Herbrüggen T, Glaser S J, Bergholm V, Storcz M J, Ferber J and Wilhelm F K 2007 *Phys. Rev. A* **75** 012302

[38] Grigorenko I A and Khveshchenko D V 2005 *Phys. Rev. Lett.* **95**, 110501

[39] Schulte-Herbrüggen T, Spörl A, Khaneja N and Glaser S J 2006 Optimal control for generating quantum gates in open dissipative systems *Preprint* quant-ph/0609037

[40] Hohenester U 2006 *Phys. Rev.* B **74** 161307

[41] Kosut R L, Grace M, Brif C and Rabitz H 2006 On the distance between unitary propagators of quantum systems of differing dimensions *Preprint* quant-ph/0606064

[42] Reimpell M and Werner R F 2005 *Phys. Rev. Lett.* **94** 080501

[43] Kosut R L and Lidar D A 2006 Quantum error correction via convex optimization *Preprint* quant-ph/0606078

[44] Childress L, Gurudev Dutt M V, Taylor J M, Zibrov A S, Jelezko F, Wrachtrup J, Hemmer P R and Lukin M D 2006 *Science* **314** 281

[45] Coish W A, Golovach V N, Egues J C and Loss D 2006 *Phys. Stat. Sol. B* **243** 3658
Coish W A and Loss D 2004 *Phys. Rev.* B **70** 195340

[46] Gilchrist A, Langford N K and Nielsen M A 2005 *Phys. Rev.* A **71** 062310

[47] Phoenix S J D and Knight P L 1991 *Phys. Rev. Lett.* **66** 2833

[48] Reed M and Simon B 1980 *Methods of Modern Mathematical Physics, Vol. 1: Functional Analysis* (New York: Academic Press)

[49] Yip F, Mazziotti D and Rabitz H 2003 *J. Chem. Phys.* **118** 8168

[50] Ramakrishna V, Salapaka M V, Dahleh M, Rabitz H and Peirce A 1995 *Phys. Rev.* A **51** 960
Turinici G and Rabitz H 2001 *Chem. Phys.* **267** 1

[51] Kraus K 1983 *States, Effects and Operations: Fundamental Notions of Quantum Theory* (Berlin: Springer-Verlag)
Alicki R and Lendi K 1987 *Quantum Dynamical Semigroups and Applications* (Berlin: Springer-Verlag)

[52] Rabitz H, Hsieh M and Rosenthal C 2005 *Phys. Rev.* A **72** 052337

[53] Brif C, Rabitz H, Hsieh M, Walmsley I and Kosut R 2006 Robustness of optimally controlled unitary quantum operations (unpublished)

[54] Mitra A and Rabitz H 2003 *Phys. Rev.* A **67** 033407

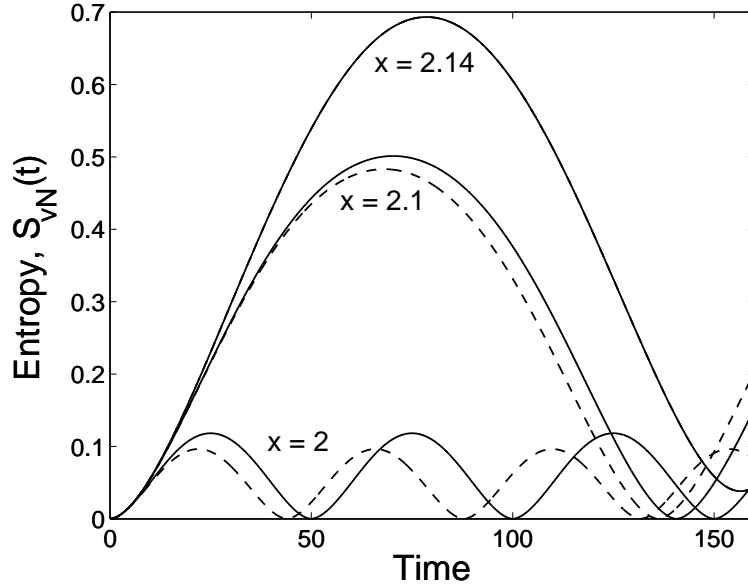[55] Rothman A, Ho T S and Rabitz H 2005 *Phys. Rev.* A **72** 023416
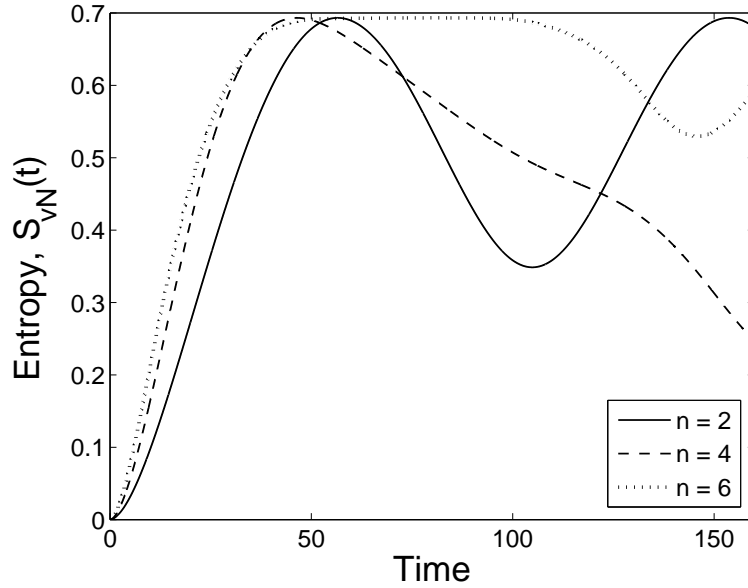
Figure 1. The time-evolution of the entropy $S_{\mathrm{vN}}(t)$ for the uncontrolled system of one qubit coupled to a one-particle environment, with $\gamma = 0.02$, $\omega_1 = 1$, and various values of ω_2. Solid lines: $\omega_2 = (\pi - x)^{-1}$; dashed lines: $\omega_2 = \pi - x$ (with $x = 2, 2.1, 2.14$). The initial state is $|\Psi_0\rangle$ of (19). For a given value of γ, closer frequencies ω_1 and ω_2 enhance the interaction between the qubit and environment, causing stronger decoherence and longer revival times.

Figure 2. The time-evolution of the entropy $S_{\mathrm{vN}}(t)$ for the uncontrolled systems of one qubit coupled to n-particle environments: $n = 2$ (solid line), $n = 4$ (dashed line), and $n = 6$ (dotted line). The coupling constant is $\gamma = 0.02$. Frequencies of the qubit, ω_1, and the environmental particles, ω_j $(j = 2, \ldots, n + 1)$, are given by (23). The initial state is $|\Psi_0\rangle$ of (19).
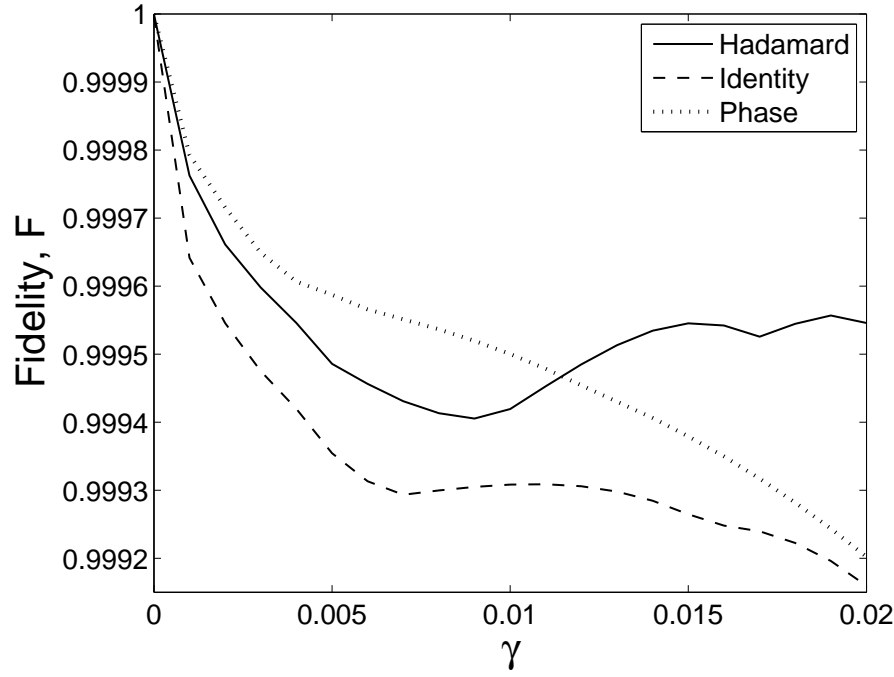
Figure 3. The gate fidelity F versus the coupling constant γ, for optimally controlled one-qubit gates: Hadamard (solid line), identity (dashed line), and phase (dotted line). Each one-qubit gate is coupled to a one-particle environment. Values of γ range from 0 to 0.02 in increments of 0.001.
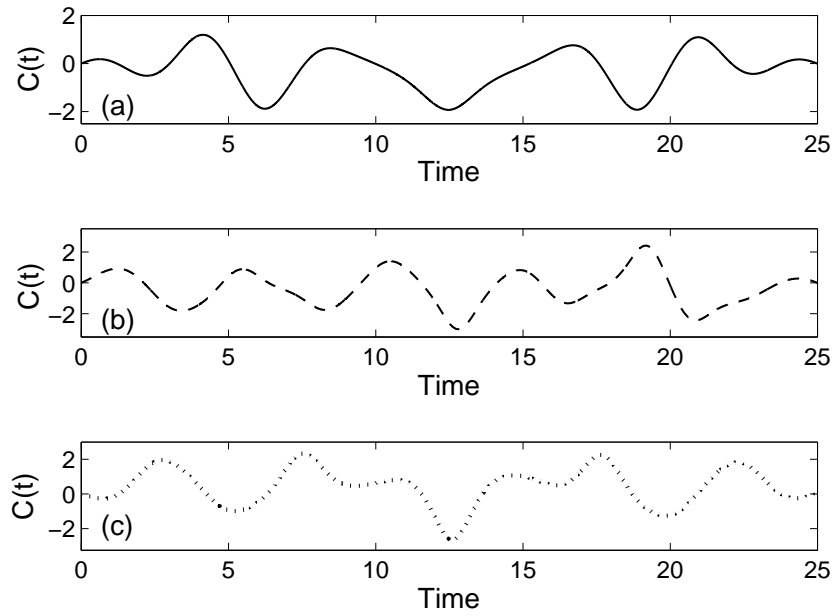

Figure 4. Optimal control fields $C(t)$ versus time, for one-qubit gates: (a) Hadamard, (b) identity, and (c) phase. Each one-qubit gate is coupled to a one-particle environment ($\gamma = 0.02$).
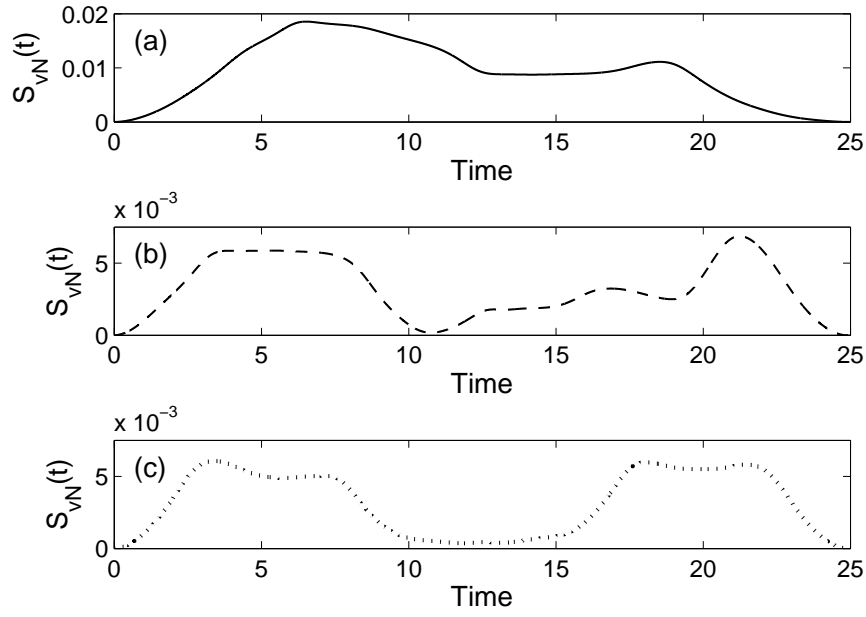
Figure 5. The von Neumann entropy $S_{\mathrm{vN}}(t)$ versus time, for optimally controlled one-qubit gates: (a) Hadamard, (b) identity, and (c) phase. Each one-qubit gate is coupled to a one-particle environment ($\gamma = 0.02$). The initial state is $|\Psi_0\rangle$ of (19).
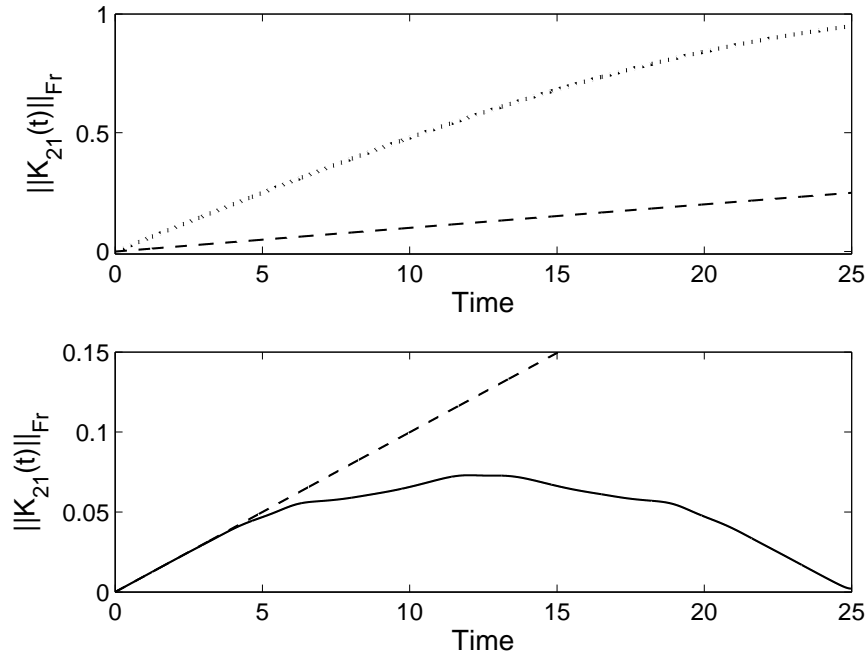
Figure 6. The time-evolution of the Kraus operator's norm, $\|K_{21}(t)\|_{\mathrm{Fr}}$, for the system of one qubit and one environmental particle: uncontrolled evolution with $\gamma = 0.1$ (dotted line), uncontrolled evolution with $\gamma = 0.02$ (dashed lines), and controlled evolution, under the optimal control field generating the Hadamard gate, with $\gamma = 0.02$ (solid line). The initial state is $|\Psi_0\rangle$ of (19).
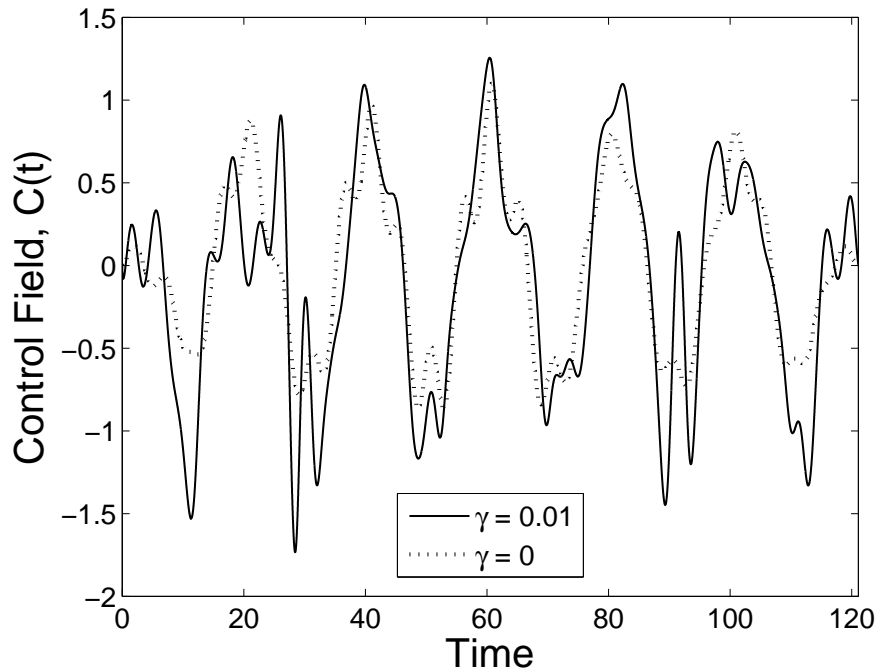

Figure 7. Optimal control fields $C(t)$ versus time, for the two-qubit CNOT gate with $\gamma = 0.01$ (solid line) and $\gamma = 0$ (dotted line).
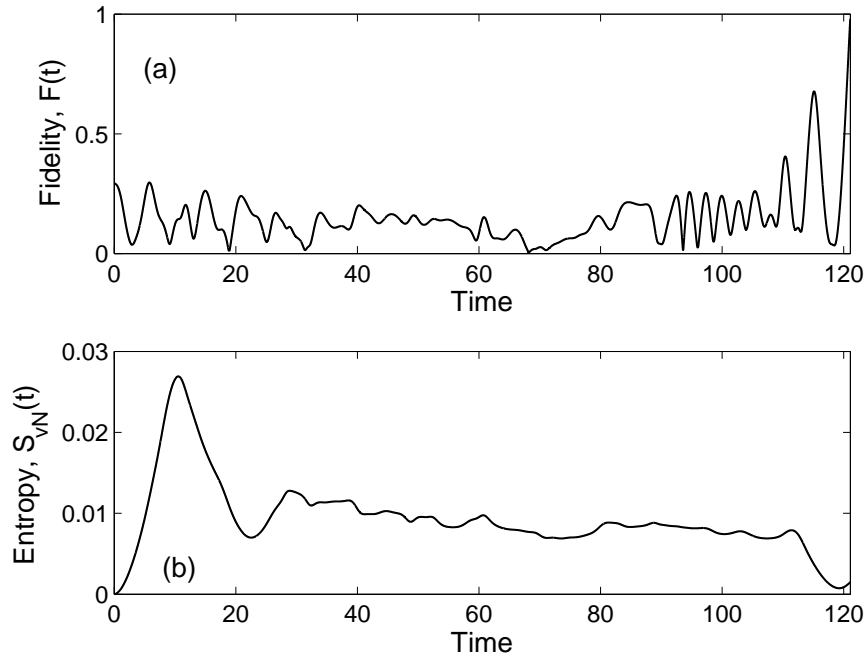
Figure 8. The time-evolution of (a) fidelity $F(t)$ and (b) von Neumann entropy $S_{\mathrm{vN}}(t)$ during the optimally controlled CNOT gate operation ($m = 2$, $n = 1$, and $\gamma = 0.01$). These results demonstrate that a high degree of coherence (quantified by the entropy) does not ensure a correspondingly high value of the gate fidelity. The initial state for the entropy computation is $|\Psi_0\rangle$ of (19).
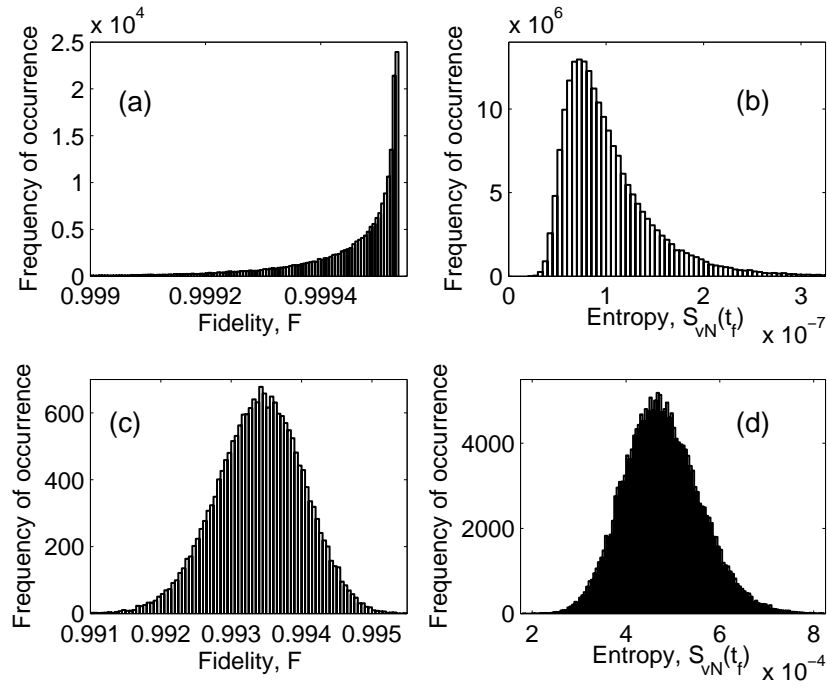
Figure 9. Frequency histograms for the gate fidelity and final-time entropy distributions, obtained when the control field optimized for the Hadamard gate with $\gamma = 0.02$ is applied to an ensemble of systems with normal variations in the coupling constants γ_{ij}. The distribution for each non-zero γ_{ij} is normal with a mean $\overline{\gamma} = 0.02$ and a standard deviation $\sigma_\gamma = \overline{\gamma}/8 = 0.0025$. Sub-plots include frequency histograms of (a) the fidelity distribution for $n = 1$, (b) the entropy distribution for $n = 1$, (c) the fidelity distribution for $n = 4$, and (d) the entropy distribution for $n = 4$. Note the axes scale differences in the sub-plots. Table 2 reports statistical data for these distributions.
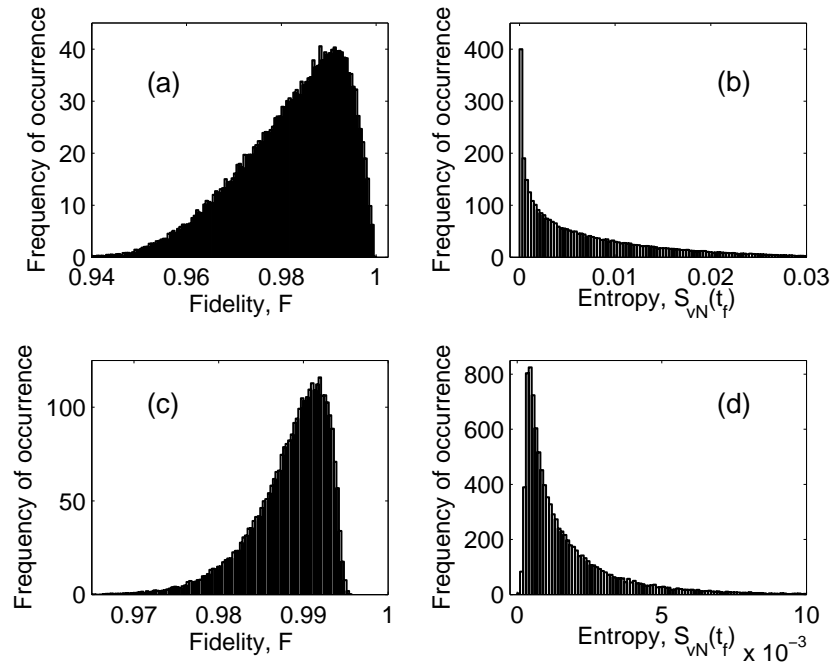
Figure 10. Frequency histograms for the gate fidelity and final-time entropy distributions, obtained when the control field optimized for the Hadamard gate with transition frequencies ω_i given by (22) for $n = 1$ and (23) for $n \geq 2$ is applied to an ensemble of systems with normal variations in the transition frequencies. The distribution for each transition frequency is normal with a mean $\overline{\omega}_i = \omega_i$ and a standard deviation $\sigma_{\omega_i} = \omega_i/25$. Sub-plots include histograms of (a) the fidelity distribution for $n = 1$, (b) the entropy distribution for $n = 1$, (c) the fidelity distribution for $n = 4$, and (d) the entropy distribution for $n = 4$. Note the axes scale differences in the sub-plots. Table 2 reports statistical data for these distributions.